Energetics of Interfacial Interactions of Hydrocarbon Fluids with Kerogen and Calcite using Molecular Modeling

Zelong Zhang,*[,†] Haoran Liu, [‡,⊥] and Jianwei Wang[†,§]

[†]Department of Geology and Geophysics, Louisiana State University, Baton Rouge, LA 70803, United States

[‡]Department of Experimental Statistics, Louisiana State University, Baton Rouge, LA 70803, United States

[⊥]Department of Oceanography and Coastal Sciences, Louisiana State University, Baton Rouge, LA 70803, United States

[§]Center for Computation and Technology, Louisiana State University, Baton Rouge, LA 70803, United States

Corresponding to: zelongz@lsu.edu

Abstract

Understanding the fluid-rock interactions is essential to characterize the behavior of petroleum fluids in reservoir formations. Such understanding is often difficult to obtain due to the heterogeneous nature of hydrocarbon systems. This study investigated the interactions of light oil molecules with calcite and kerogen using Molecular Dynamics simulations. Specifically, octane and octanthiol were used as model molecules for non-polar and polar oil compounds; a kerogen fragment molecule as the building block for kerogen, the major constituent of reservoir rock organics; calcite as a model system for hydrophilic materials in reservoir rocks. The Umbrella Sampling method combined with Weighted Histogram Analysis Method was employed to calculate the free energy profiles of oil molecule desorption from kerogen and calcite surfaces. The effects of oil molecular polarity, size of oil molecular cluster, and the presence of water on the interfacial interactions were evaluated based on the free energy profile of desorption. The results show the free energy of desorption of oil molecules is significantly reduced at both kerogen and calcite surfaces if water is presented. For the polar oil molecule, the free energy of desorption is higher than that of non-polar oil at both calcite and kerogen surfaces. The kerogen surface exhibits stronger binding energies of oil molecules than the calcite. These findings suggest that 1) polar oil compounds require more effort to be recovered than non-polar ones from the reservoir rocks, 2) isolated oil molecules or oil clusters of a smaller size are harder to be displaced from the surfaces than a larger size of molecular clusters, and 3) the presence of water decreases the free energy of desorption at both surfaces. The results provide an energetic perspective of the interfacial interactions for the oil recovery in reservoir formations. The methodology presented in this study demonstrates that the MD simulation is capable to evaluate the impact of different factors on the interfacial interactions for the fundamental understanding of the oil recovery processes in petroleum reservoirs, which can provide valuable implications for developing novel technologies of oil recovery.

41

TOC

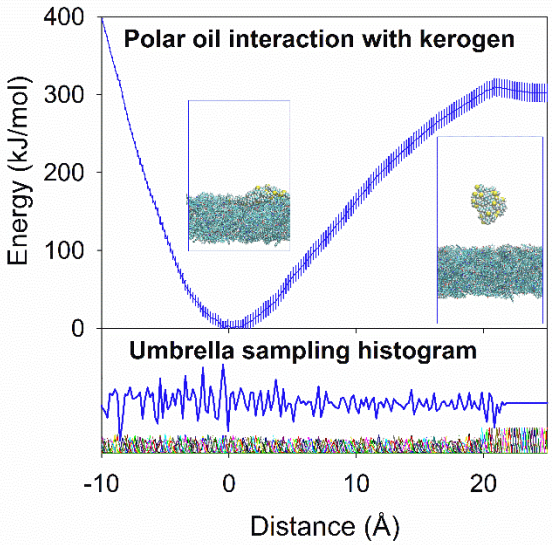
Polar oil interaction with kerogen
Umbrella sampling histogram
Energy (kJ/mol)
400
300
200
100
0
-10
0
10
20
Distance (Å)

42

1 Introduction

Oil is the main energy source for our modern civilization and will remain as a major contributor of global energy in the foreseeable future.[1] However, only a portion of oil preserved in a reservoir can be recovered. Thus, it is imperative to improve the recovery efficiency of petroleum reservoirs. Current methods to improve oil production including primary, secondary, and tertiary oil recovery techniques can yield 30 to 60 % of the original oil in place, successively. Hence, up to 70% of the original oil in place is still left within a reservoir.[1,2]

The pressing demand of energy from modern civilization has spurred technical innovations to improve oil recovery, especially through tertiary oil recovery or enhanced oil recovery. However, there is a limited understanding of how hydrocarbon-bearing fluids interact with the materials in reservoir formations. This knowledge gap impairs the assessment of the economic potential of a hydrocarbon reservoir. For example, relative permeability, an essential parameter of fluid flow characteristics for formation evaluation, is measured by Special Core Analysis (SCAL) through conducting flow experiments on core plugs taken from a reservoir. However, SCAL results are often contradictory or cannot be properly implemented in the reservoir modelling and petrophysical evaluation.[3–5] A myriad of factors may complicate the results, including the hydrofracture geometries, networks of preexisting fractures, adsorption and desorption processes, non-Darcy multiphase flow, chemically and structurally heterogeneous formations, etc.[6]

The interfacial interactions between the fluid and rock play a key role in all these complications. As shown in Figure 1, if a pore has less than 100 nm radius and the intramolecular interaction has an effective distance of 3 nm, a significant portion (12% – 100% volume) of confined fluid can be directly affected by the interfacial interactions. Therefore, to

66 further improve recovery efficiency, a fundamental understanding of the fluid-rock interactions
67 is essential.

68 To probe the interfacial interactions at nanoscales, molecular-level characterization is
69 necessary. Both experimental and computational approaches have been applied to study the
70 hydrocarbon fluid behavior in the rock at nanoscale. Extensive experimental studies have been
71 conducted on the reservoir formations to characterize the organic content[7,8], pore structure[9–12],
72 and petrophysical properties[11,13–15]. These studies aimed to calibrate the empirical models in
73 reservoir engineering to describe the fluid flow[16,17] and to provide a basis for reservoir
74 assessment and production optimization.[18] However, due to the compositional and structural
75 heterogeneity of reservoir formations, it is challenging to interpret the dynamics and kinetics of
76 interface interactions without knowing the molecular scale details. Current understanding of the
77 hydrocarbon systems heavily relies on the characterization technologies to conduct experiments
78 on surfaces and interfaces[19–21] such as Focus Ion Beam Scanning Electron Microscopy (FIB-
79 SEM),[15,22,23] Transmission Electron Microscopy (TEM),[23,24] Atomic Force Microscopy
80 (AFM),[16,25,26] X-ray Diffraction (XRD),[27,28] X-ray microtomography (Micro-CT),[29,30] Nuclear
81 Magnetic Resonance (NMR),[31,32] etc. Implementing these methodologies to characterize
82 microscopic phenomena becomes challenging at the molecular level. Unlike experiments,
83 computational simulations can study physical phenomena over a range of scales,[33] directly
84 connecting the microscopic details of a system to macroscopic properties of experimental
85 interest.[34] Due to the intensive computation, Quantum Mechanics (QM) simulations have strict
86 limits on the size, time, and complexity of the systems.[33–35] Molecular simulations, built on
87 classical molecular mechanics (MM) such as Monte Carlo (MC) and Molecular Dynamics (MD),
88 are more appropriate than QM methods to address the issues of size and complexity of the

hydrocarbon systems. MC methods are stochastic approach, suitable for system equilibrium, while MD techniques are deterministic, suitable for both equilibrium and transport properties of a given system.[34,35] Thus, this study used MD to investigate the energetics of fluid-rock interactions. Currently, there are several studies using MD to investigate hydrocarbon fluid interactions with minerals and kerogen, such as 1) the adsorption, diffusion, and permeation of hydrocarbon fluid in shale kerogen and kerogen analogue;[36–43] 2) slippage, displacement, and adsorption of hydrocarbon flow on quartz, calcite slits, and montmorillonite slits;[44–47] 3) detachment of oil cluster from silicate surfaces in surfactant solution.[48] These studies evaluated the effect of nanopores on the properties of hydrocarbon fluid, such as bulk viscosity, contact angle, and slippage with focuses on the phenomena of the interactions. For instance, Liu et al 2012 stated that water can penetrate the oil—water interface and form a surface water layer on a hydrophilic silica surface, enhancing the oil detachment from the hydrophilic surface.[48] However, there is a knowledge gap in the energetic aspect of the interactions, which is essentially underexplored. This lack of the knowledge on the thermodynamics of the interactions limits a fundamental understanding of hydrocarbon fluids interactions with reservoir formations.

The present study attempts to examine the feasibility of the computational approach to evaluate the free energy profile of oil compounds desorption from the surfaces of reservoir rock materials. The methods for calculating free energy profile by Umbrella Sampling, widely used in computational biology and biochemistry[49], were adopted to compute the free energy changes of the oil interactions with the rock materials in the desorption. We examined the surfaces of kerogen and calcite to evaluate the effect of four different variables including oil polarity (polar vs non-polar oil), oil cluster size (a single molecule oil vs 30 molecules oil cluster), surface hydrophobicity (inorganic calcite mineral vs organic kerogen), and surface water (the presence

vs the absence of surface water). Probing the free energy changes in oil-rock interactions can provide fundamental understanding of the thermodynamics of the surface wettability and hydrocarbon behaviors in reservoir formations.

2 Method

2.1 Molecular models for oil, kerogen, and calcite

Crude oil is a mixture of widely varying polar and non-polar compounds as well as their proportions, composition, and molecular weight. Typically, crude oil contains over 45% non-polar (e.g. alkanes and cycloalkanes) and less than 15% polar species (e.g. N-, S-, O- and metal-containing compounds).[50,51] Polar components can significantly affect properties of hydrocarbon fluid in reservoir such as viscosity, contact angle, interfacial activity, emulsion, and chemical stability.[52–54] The oil-rock interactions are largely attributed by the polar species,[55] particularly in organic phases which usually retain more polar components than minerals[52]. Thioalkanes are common sulfur compounds found in crude oils.[56] Crude oil, especially from shale, can has a high content of light oil (C_1-C_9).[57,58] Therefore, we selected 1-octanethiol ($C_8H_{18}S$) with a dipole moment of 2.9 D[59] and its non-polar counterpart n-octane (C_8H_{18}) as the models for polar and nonpolar oil respectively in our simulations as shown in Figure 2. In addition, to model a small oil drop, we prepared two oil clusters consisted of 30 molecules of octanethiol and octane for polar and non-polar oil droplets respectively as shown in Figure 3(c).

Reservoir rocks are highly complicated by complex microstructures and mineralogy as well as various amount of inorganic and organic constituents. Major mineral phases include clays, quartz, and carbonates (calcite and dolomite).[60] Due to its simple structure and ubiquitous

presence in formation rocks, we chose the calcite (104) face as a mode for hydrophilic surface of reservoir rocks. The calcite (104) is a flat stoichiometric surface, which is one of most common mineral faces occurred in both geological and biological systems and has been well studied both computationally and experimentally.[61] The key organic phase in shale involved in the interactions with hydrocarbon fluid is kerogen.[52,62,63] Despite the complexity of kerogen in reservoir formations[64], many studies used graphene to represent kerogen[36,42,43,65–68]. The differences between graphene and kerogen, such as bonding environment of functional groups[69,70] and surface morphology[64], give rise to different chemical and mechanical properties and interfacial interactions, resulting in inadequate models and unrealistic results with respect to experimental measurements[70,71]. To reasonably capture fundamental properties of kerogen, we employed a molecular fragment $C_{22}H_{13}ON$ directly derived from type II kerogen to build kerogen surfaces,[37] which is the most common kerogen in hydrocarbon-bearing shale formations.[64] The kerogen molecule has five benzene rings, a secondary amine, and a phenol group, resulting a polar compound. To create kerogen surfaces, 511 kerogen molecules were randomly added into a computational supercell (18,907 atoms in total), quenched from 3000 to 300 K. The surface was then created by inserting a vacuum space between the kerogen and lastly a stabilization and a relaxation of the surface were followed at 300 K using an NVT ensemble.

The calcite (104) surface in Figure 3(b) was built with 1620 $CaCO_3$ molecule units with a dimension of approximately 7 × 7 × 2 nm with 8,100 atoms. The kerogen surface in Figure 3(a) was built with 511 $C_{22}H_{13}ON$ molecule units with a dimension of approximately 8 × 8 × 3 nm and 18,907 atoms as shown. Because of the ubiquitous presence of water in the reservoir formations, water molecules were added to the fluid. To ensure the oil molecules surrounded by water, 7,250 and 10,000 water molecules were added to the calcite surface of single oil molecule

157 or oil cluster, respectively; while 7,500 and 10,000 water molecules were placed on kerogen
158 surfaces of single oil molecule or oil cluster, respectively.

159 A previous experimental study indicates the calcite (104) surface exhibits neutral charge
160 due to the stoichiometry and alternating of Ca^{2+} and CO_3^{2-}.[72,73] Kerogen surfaces can be
161 negatively charged due to the deprotonation of functional groups, such as OH and NH. However,
162 classical MD models only simulate interatomic interactions by empirical potentials for bond
163 length, angle, and dihedral, whereas formation and breaking of covalent bonds are not considered
164 unless specified by force field. Both calcite and kerogen surfaces maintain electrical neutrality
165 owing to the charge balance of each model molecule. Layers of alternating Ca^{2+} and CO_3^{2-} on the
166 calcite (104) create a flat surface, while the benzene rings and polar functional groups of kerogen
167 molecule yield a highly heterogenous surfaces of kerogen.

168

169 2.2 Molecular Dynamics (MD) Simulation and Gibbs Free Energy Profiles

170 MD simulations in this study were deployed using software package GROningen
171 MAchine for Chemical Simulations (GROMACS).[74] All simulations were employed the three-
172 dimensional periodic boundary conditions. The OPLS-AA force field was used to describe oil
173 molecules and kerogen.[75] The SPC potential is used to describe water molecule.[76] A previously
174 developed force field was used for calcite.[77] All these potentials have been tested and are capable
175 of producing satisfactory results on bulk and interfacial properties, which are consistent with
176 experimental data.[78–80] Newton's equations of motion were integrated using the leap-frog scheme
177 with a timestep of 1 fs, fast Smooth Particle-Mesh Ewald (SPME) electrostatics, Verlet cutoff-
178 scheme, and temperature coupling using a Nose-Hoover extended ensemble with a coupling

constant of 0.1 ps. Simulations were visualized by Visual Molecular Dynamics (VMD) package.[81]

The potential of mean force for the oil interactions with different surfaces was computed by Umbrella Sampling and the Weighted Histogram Analysis Method (WHAM).[82,83] Gromacs package was used to carry out Umbrella Sampling simulations by running separate simulation windows along the reaction coordinate individually. The simulation windows were generated by simulations pulling the oil into or away from the surfaces regardless of the presence of water.

In each simulation window, umbrella potential, a biased harmonic potential, was applied to the system. For each individual simulation window, we first applied a constraint potential with a force constant 9000 $kJ \cdot mol^{-1} \cdot nm^{-1}$ for 0.1 ns to equilibrate the system, then deployed an umbrella potential with a force constant 9000 $kJ \cdot mol^{-1} \cdot nm^{-2}$ for 0.1 ns up to 0.2 ns to obtain probability distribution of the given reaction coordinate. With enough sampling overlaps between simulation windows in the entire reaction coordinate space, a free energy profile curve can be calculated by combining data from each window using WHAM.[82,84]

A analysis routine to estimate the errors of the energy profiles was developed using LOESS algorithm in RStudio.[85,86] This method takes the energy profile and employs the bootstrap technique to calculate the confidential intervals at 95% confidence level. The computed errors are listed as shown in Table 1 denoted by brackets. The fluctuation of free energy profile as shown in Figure S1 is consistent with the size of the estimated error bar.

3 Results

Free energy surfaces in Figures 4-7 show how the system energy changes as a function of the distance between oil compounds and surfaces. When the oils molecules are close to the surfaces, the energy increases due to repulsive interactions. When the oils gradually move away from the surface, the energy first reaches the minimal point, at which point the adsorption occurs at the surfaces. An absence of the minimum suggests zero desorption energy. As the distance continuously increases, the energy increase until the system reaches the energy plateau where no additional energy is required to desorb the oil molecules from the surfaces.

3.1 Interactions of oil molecules with kerogen surface

The free energy profiles in Figure 4 and Table 1 show the energy changes as a function of the distance between oil compounds and kerogen surface in the presence of water. The desorption energies are 17.0 ± 2.0 kJ/mol and 16.5 ± 3.3 kJ/mol for non-polar and polar single oil molecule and 371± 12.4 kJ/mol and 209 ± 7.0 kJ/mol for non-polar and polar oil clusters, respectively. In the absence of water, it is challenging to maintain oil molecules as a cluster at or above 300 K. To stabilize the oil cluster, a series of Umbrella Sampling simulations were carried out under lower system temperatures to extrapolate the desorption energy to 300 K (detail was discussed in Figure S3). The desorption energies of the oil clusters on kerogen surfaces are 437 ± 13.5 kJ/mol for both polar and non-polar (Figure S3). For the single oil molecule, the desorption energies on kerogen in Figure 5 and Table 1 are 23.3 ± 3.5 kJ/mol and 39.5 ± 9.5 kJ/mol for non-polar and polar, respectively.

3.2 Interactions of oil molecules with calcite (104) surface

The free energy profiles in Figure 6 shows how free energy changes as a function of the distance between oil compounds and the calcite (104) surface in water. Unlike the rest free energy profiles (described later), they exhibit a distinct pattern: as the distance increase, the free energy quickly decreased and then maintained at the same value as the molecule is further away from the surface. Such patterns indicate near zero energy of the desorption of oil molecules on the calcite surface in the presence of water.

For comparison, the same systems without water were simulated, of which the free energy profiles are depicted in Figure 7. The results show that 33.6 ± 3.9 kJ/mol and 18.0 ± 5.5 kJ/mol are required to desorb polar and non-polar oil molecules from the calcite surfaces respectively, and 222 ± 36 kJ/mol and 198 ± 42 kJ/mol to desorb polar and non-polar oil clusters, respectively. A detailed analysis of the trajectory (Figure S4) suggests that the polar molecule was bound to the calcite surface through the thiol functional group –SH, which confirms a previous study on the adsorption of simple organic molecules on calcite (104).[87] In addition, the thiol group –SH of polar oil appears to favor the sites of Ca^{2+} site of calcite (104) surface, whereas the non-polar oil shows no preference of absorption sites.

4 Discussion

4.1 Effect of surface composition on the desorption energy

Our study shows that in general oil molecules have stronger interactions with kerogen than with calcite regardless of surface environment and oil molecular polarity. Kerogen is organic compound and usually oleophilic. The surface property depends on the specific functional groups. The kerogen model in this study contains functional groups such as hydroxyl

and sulfhydryl groups (giving rise to thiols), which inherently exhibits a strong affinity with hydrophilic surfaces while the rest strongly interacts with hydrophobic surfaces. On the other hand, calcite, especially the (104) face, is strongly hydrophilic with ionic species Ca^{2+} and CO_3^{2-} on the surface. Therefore, water is more easily to be desorbed from the kerogen surface than from the calcite surface, leading to higher desorption energy for oil molecules at the kerogen surface and weak desorption at the calcite surface. Another factor that contributes to the difference between kerogen and calcite is the surface area. Calcite has a low surface area which weakens its sorption capacities.[88] On the other hand, kerogen is porous and waxy according to experimental observations.[64,89] The effective surface area on kerogen would be much higher than calcite, leading to a higher desorption capacities for oil.

As a result of their different surface properties, the desorption energy at kerogen surface is 5.3 to 17 kJ/mol higher for a single oil molecule and 210 to 372 kJ/mol higher for the oil cluster (7.0 to 12.4 kJ/mol per molecule for the oil cluster) than at the calcite surface. The difference in the desorption energies of both single molecule oil and oil cluster implies that oil recovery from organic phases of reservoir rock can take more energy than from these highly hydrophilic surfaces of inorganic mineral phases such as calcite.

4.2 Effect of molecular polarity

Our study shows that the polar oil has a stronger interaction with the kerogen and calcite surfaces than non-polar oil. At kerogen surface, molecular polarity plays an imperative role in the energetics of the oil desorption. These phenomena can be explained by the dipole interactions. Since there is no free ion in the systems, the intermolecular interactions are

dominated by permanent dipole interaction, or Keesom interaction. As shown in Figure S5 a and c, the thiol functional group (–SH, yellow) of the polar oil tend to be in proximity to the functional groups of kerogen molecules such as amine (–NH–, blue) and hydroxyl (–OH, red) upon contact at the interface, which confirms the expected dipole interactions. Unlike the polar oil, non-polar oil molecules have no dipole moment, therefore a weaker desorption energy than the polar oil molecules is expected. Thus, the interactions of the polar oil molecule with kerogen surface is stronger than that of non-polar.[90] As shown in the Table 1, the desorption energies of the single molecule oil show that the polar oil molecule requires energy about two times of the energy of non-polar per molecule in the absence of water. The desorption energies of single polar and nonpolar oil molecules are approximately the same in the presence of water. For the oil cluster, our calculation indicates that polar oil cluster requires the similar desorption energies as the non-polar oil cluster. These results suggest that the effect of polarity is complicated by kerogen surface property and the presence of water.

At the calcite (104) surface, polar oil molecules consistently require higher desorption energies than its counterpart non-polar oil owing to the molecular dipole of the polar oil and the hydrophilic nature of the calcite surface. Although previous studies suggested that calcite (104) is overall non-polar because the alternating Ca^{2+} and CO_3^{2-} are closely packed and charge balance is maintained,[91,92] the electrostatic interaction between ionic species at the calcite surface and the functional group at the polar molecule favors the adsorption of the polar oil molecules. Therefore, the desorption energy for the polar oil molecule is about two times of the desorption energy for the non-polar oil molecule and the desorption energy for the polar oil molecular cluster is about 10% higher than the desorption energy for the non-polar oil cluster in the absence of water.

289

290 4.3 Effect of surface water

291 Our study shows that the presence of surface water reduces the oil desorption energy on
292 all surface conditions, promoting the oil desorption in all the cases. As discussed previously, the
293 calcite surface is hydrophilic, while kerogen is both hydrophilic and hydrophobic. The surface
294 water can easily be attracted to the calcite surface and kerogen hydrophilic functional groups.
295 Both water and polar oil molecules have similar dipole moments 2.9 D and 2.27 D,[59,76]
296 respectively. Water molecules compete with polar oil molecules for adsorption at surfaces with a
297 hydrophilic character, and consequently reducing the desorption energy of the oil molecules at
298 the surfaces. The interactions of waters with the calcite (104) surfaces were much stronger than
299 with kerogen surfaces, suggesting a weaker hydrophilic nature of kerogen surface than the calcite
300 surface. The affinity between calcite and water is stronger than that between calcite and oil,
301 resulting in a strong oil-repellent surface of calcite in the presence of water. As shown in Table
302 1, kerogen surface with water requires much lower energies to desorb oil. For polar oil, the
303 surface water brought a reduction of 50% - 60% on desorption energy to desorb polar oil
304 compound and 15% - 30% reduction for non-polar oil compound. The energy differences
305 between non-polar and polar oil also demonstrate the crucial role of molecular polarity on the
306 fluid-rock interactions. Given the strong hydrophilicity of calcite, the calcite surface becomes
307 oleophobic, jettisoned all the surface oil, in the presence of water. The result provides a
308 fundamental understanding of the role of water in interactions of oil molecules and reservoir
309 materials and in oil recovery.

310

311 4.4 Effect of oil clustering

312 Our study shows that oil clusters of require lower desorption energies per molecule than a
313 single oil molecule. For instance, the desorption energy of a single molecule of polar oil is 4.6 to
314 25.2 kJ/mol higher than the desorption energy per molecule of the oil cluster, which is 37% to
315 340% increase of desorption energy per molecule of the oil cluster. This difference can be
316 mainly attributed to the number of oil molecules that directly interact with the surface. Not all
317 the molecules in the 30-molecule clusters directly interact with the surfaces, while the single
318 molecule always interacts with the surfaces, which leads to the smaller desorption energies per
319 molecule. Although the oil molecular clusters are still too small to compare with oils in the
320 porous medium in reservoir rocks, the trend quantified in this study suggests that as the pore size
321 decreases, recovering the oil confined in the pores becomes more challenging.

322

323 **5 Concluding remarks and implications**

324 This study demonstrated that Molecular Dynamics simulation is capable of calculating
325 the free energy surface of desorption of single oil molecules and oil molecular clusters at calcite
326 and kerogen surfaces. The results provide fundamental understandings of the interfacial
327 interactions and valuable implications for oil recovery in reservoirs. The main conclusions are as
328 follows.

329 (1) Hydrophobicity of the surface of reservoir materials has a significant effect on the
330 desorption of the oil molecules from the surfaces, leading to a higher free energy cost for
331 oil displacement from organic phases of reservoir rock than from the highly hydrophilic
332 surfaces of inorganic mineral phases such as calcite.

(2) The polarity of oil molecules strongly affects the interfacial interactions at both the kerogen and calcite surfaces. The polar oil molecules require more energy to be recovered from both surfaces than non-polar ones. For complex hydrocarbon fluid systems, a large fraction of polar compounds in the oil poses a great challenge. In order to effectively model the interactions between oil and the reservoir materials and to produce reliable results, an accurate description of the polarity of oil molecules is necessary.

(3) The presence of water at interface plays a fundamental role in the interactions between oil molecules and reservoir materials. Because of its large dipole moment, water facilitates the oil desorption by interacting with hydrophilic surfaces or sites of either organic kerogen or inorganic minerals.

(4) Single oil molecule or small oil molecule cluster dispersed in small nanopores tend to be more challenging to be recovered than large oil molecular clusters due to the stronger interactions of oil molecules with the surfaces.

The success of implementing the free energy methods to study the simple hydrocarbon fluid systems paves the way for simulating more realistic and complex systems by varying temperatures, adding fluid components (e.g. electrolytes, methane, carbon dioxide, and large oil compounds) and introducing other major inorganic phases such as clay minerals and quartz.

Conflicts of interest

There are no conflicts to declare.

Acknowledgements

This research used resources of the National Energy Research Scientific Computing Center (NERSC), a U.S. Department of Energy Office of Science User Facility operated under Contract No. DE-AC02-05CH11231. Portions of this research were conducted with high performance computing resources provided by Louisiana State University (http://www.hpc.lsu.edu).

References

(1) EIA. *Annual Energy Outlook 2019*; AEO2019; U.S. Energy Information Administration: Washington, DC, 2019.

(2) Thomas, S. Enhanced Oil Recovery - An Overview. *Oil Gas Sci. Technol. - Rev. IFP* **2008**, *63* (1), 9–19. https://doi.org/10.2516/ogst:2007060.

(3) Forbes, P. The Status of Core Analysis. *J. Pet. Sci. Eng.* **1998**, *19* (1), 1–6. https://doi.org/10.1016/S0920-4105(97)00030-2.

(4) Gao, B.; Kralik, J.; Vo, L.; Shebl, H.; Al Shehhi, R.; Al Jawhari, M. O.; Fullmer, S. State of the Art Special Core Analysis Program Design and Results for a Middle Eastern Carbonate Reservoir; Society of Petroleum Engineers, 2015. https://doi.org/10.2118/177510-MS.

(5) van der Weerd, H.; Masalmeh, S. K.; Jing, X. D.; van Vark, W.; Christiansen, S.; Van Dorp, J. Impact of SCAL (Special Core Analysis) on Carbonate Reservoirs: How Capillary Forces Can Affect Field Performance Predictions. *Petrophysics* **2004**, *45* (05).

(6) Cueto-Felgueroso, L.; Juanes, R. Forecasting Long-Term Gas Production from Shale. *Proc. Natl. Acad. Sci.* **2013**, *110* (49), 19660. https://doi.org/10.1073/pnas.1319578110.

(7) Zhang, T.; Ellis, G. S.; Ruppel, S. C.; Milliken, K.; Yang, R. Effect of Organic-Matter Type and Thermal Maturity on Methane Adsorption in Shale-Gas Systems. *Org. Geochem.* **2012**, *47*, 120–131. https://doi.org/10.1016/j.orggeochem.2012.03.012.

(8) Hutton, A. C.; Kantsler, A. J.; Cook, A. C.; McKirdy, D. M. ORGANIC MATTER IN OIL SHALES. *APPEA J.* **1980**, *20* (1), 44–67. https://doi.org/10.1071/aj79005.

(9) Ross, D. J. K.; Marc Bustin, R. The Importance of Shale Composition and Pore Structure upon Gas Storage Potential of Shale Gas Reservoirs. *Mar. Pet. Geol.* **2009**, *26* (6), 916–927. https://doi.org/10.1016/j.marpetgeo.2008.06.004.

(10) Loucks, R. G.; Reed, R. M.; Ruppel, S. C.; Hammes, U. Spectrum of Pore Types and Networks in Mudrocks and a Descriptive Classification for Matrix-Related Mudrock PoresSpectrum of Pore Types and Networks In Mudrocks. *AAPG Bull.* **2012**, *96* (6), 1071–1098. https://doi.org/10.1306/08171111061.

(11) Sondergeld, C. H.; Ambrose, R. J.; Rai, C. S.; Moncrieff, J. Micro-Structural Studies of Gas Shales; Society of Petroleum Engineers, 2010. https://doi.org/10.2118/131771-MS.

(12) Clarkson, C. R.; Solano, N.; Bustin, R. M.; Bustin, A. M. M.; Chalmers, G. R. L.; He, L.; Melnichenko, Y. B.; Radliński, A. P.; Blach, T. P. Pore Structure Characterization of North American Shale Gas Reservoirs Using USANS/SANS, Gas Adsorption, and Mercury Intrusion. *Fuel* **2013**, *103*, 606–616. https://doi.org/10.1016/j.fuel.2012.06.119.

(13) Passey, Q. R.; Bohacs, K.; Esch, W. L.; Klimentidis, R.; Sinha, S. From Oil-Prone Source Rock to Gas-Producing Shale Reservoir - Geologic and Petrophysical Characterization of Unconventional Shale Gas Reservoirs; Society of Petroleum Engineers, 2010. https://doi.org/10.2118/131350-MS.

(14) Vernik, L.; Milovac, J. Rock Physics of Organic Shales. *Lead. Edge* **2011**, *30* (3), 318–323. https://doi.org/10.1190/1.3567263.

(15) Milliken, K. L.; Rudnicki, M.; Awwiller, D. N.; Zhang, T. Organic Matter–Hosted Pore System, Marcellus Formation (Devonian), PennsylvaniaGeohorizon. *AAPG Bull.* **2013**, *97* (2), 177–200. https://doi.org/10.1306/07231212048.

(16) Shabro, V.; Torres-Verdin, C.; Javadpour, F. Numerical Simulation of Shale-Gas Production: From Pore-Scale Modeling of Slip-Flow, Knudsen Diffusion, and Langmuir Desorption to Reservoir Modeling of Compressible Fluid; Society of Petroleum Engineers, 2011. https://doi.org/10.2118/144355-MS.

(17) Wu, K.; Li, X.; Wang, C.; Yu, W.; Chen, Z. Model for Surface Diffusion of Adsorbed Gas in Nanopores of Shale Gas Reservoirs. *Ind. Eng. Chem. Res.* **2015**, *54* (12), 3225–3236. https://doi.org/10.1021/ie504030v.

(18) Wang, F. P.; Reed, R. M. Pore Networks and Fluid Flow in Gas Shales; Society of Petroleum Engineers, 2009. https://doi.org/10.2118/124253-MS.

(19) Zaera, F. Probing Liquid/Solid Interfaces at the Molecular Level. *Chem. Rev.* **2012**, *112* (5), 2920–2986. https://doi.org/10.1021/cr2002068.

(20) *Surface Analysis Methods in Materials Science*; O'Connor, J., Sexton, B., Smart, R., Eds.; Springer Series in Surface Sciences; Springer-Verlag: Berlin Heidelberg, 1992.

(21) Mineralogical Society of America - Mineral-Water Interface Geochemistry http://www.minsocam.org/msa/rim/rim23.html (accessed Mar 13, 2019).

(22) Milner, M.; McLin, R.; Petriello, J. Imaging Texture and Porosity in Mudstones and Shales: Comparison of Secondary and Ion-Milled Backscatter SEM Methods; Society of Petroleum Engineers, 2010. https://doi.org/10.2118/138975-MS.

(23) Curtis, M. E.; Ambrose, R. J.; Sondergeld, C. H.; Rai, C. S. Transmission and Scanning Electron Microscopy Investigation of Pore Connectivity of Gas Shales on the Nanoscale; Society of Petroleum Engineers, 2011. https://doi.org/10.2118/144391-MS.

(24) Bernard, S.; Horsfield, B.; Schulz, H.-M.; Wirth, R.; Schreiber, A.; Sherwood, N. Geochemical Evolution of Organic-Rich Shales with Increasing Maturity: A STXM and TEM Study of the Posidonia Shale (Lower Toarcian, Northern Germany). *Mar. Pet. Geol.* **2012**, *31* (1), 70–89. https://doi.org/10.1016/j.marpetgeo.2011.05.010.

(25) Javadpour, F. Nanopores and Apparent Permeability of Gas Flow in Mudrocks (Shales and Siltstone). *J. Can. Pet. Technol.* **2009**, *48* (08), 16–21. https://doi.org/10.2118/09-08-16-DA.

(26) Javadpour, F.; Moravvej Farshi, M.; Amrein, M. Atomic-Force Microscopy: A New Tool for Gas-Shale Characterization. *J. Can. Pet. Technol.* **2012**, *51* (04), 236–243. https://doi.org/10.2118/161015-PA.

(27) Bhargava, S.; Awaja, F.; Subasinghe, N. D. Characterisation of Some Australian Oil Shale Using Thermal, X-Ray and IR Techniques. *Fuel* **2005**, *84* (6), 707–715. https://doi.org/10.1016/j.fuel.2004.11.013.

(28) Elgmati, M. M.; Zhang, H.; Bai, B.; Flori, R. E.; Qu, Q. Submicron-Pore Characterization of Shale Gas Plays; Society of Petroleum Engineers, 2011. https://doi.org/10.2118/144050-MS.

(29) Tiwari, P.; Deo, M.; Lin, C. L.; Miller, J. D. Characterization of Oil Shale Pore Structure before and after Pyrolysis by Using X-Ray Micro CT. *Fuel* **2013**, *107*, 547–554. https://doi.org/10.1016/j.fuel.2013.01.006.

(30) Duliu, O. G. Computer Axial Tomography in Geosciences: An Overview. *Earth-Sci. Rev.* **1999**, *48* (4), 265–281. https://doi.org/10.1016/S0012-8252(99)00056-2.

(31) Kadayam Viswanathan, R. K.; Cao Minh, C.; Zielinski, L.; Vissapragada, B.; Akkurt, R.; Song, Y.-Q.; Liu, C.; Jones, S.; Blair, E. Characterization of Gas Dynamics in Kerogen Nanopores by NMR; Society of Petroleum Engineers, 2011. https://doi.org/10.2118/147198-MS.

(32) Korb, J.-P.; Nicot, B.; Louis-Joseph, A.; Bubici, S.; Ferrante, G. Dynamics and Wettability of Oil and Water in Oil Shales. *J. Phys. Chem. C* **2014**, *118* (40), 23212–23218. https://doi.org/10.1021/jp508659e.

(33) Cygan, R. T. Molecular Modeling in Mineralogy and Geochemistry. *Rev. Mineral. Geochem.* **2001**, *42* (1), 1–35. https://doi.org/10.2138/rmg.2001.42.1.

(34) Allen, M.; Tildesley, D. *Computer Simulation of Liquids*, Second Edition.; Oxford University Press: Oxford, New York, 2017.

(35) Frenkel, D.; Smit, B. *Understanding Molecular Simulation: From Algorithms to Applications*, Second Edition.; Academic Press: San Diego, 2002.

(36) Falk, K.; Coasne, B.; Pellenq, R.; Ulm, F.-J.; Bocquet, L. Subcontinuum Mass Transport of Condensed Hydrocarbons in Nanoporous Media. *Nat. Commun.* **2015**, *6*, 6949. https://doi.org/10.1038/ncomms7949.

(37) Collell, J.; Galliero, G.; Gouth, F.; Montel, F.; Pujol, M.; Ungerer, P.; Yiannourakou, M. Molecular Simulation and Modelisation of Methane/Ethane Mixtures Adsorption onto a Microporous Molecular Model of Kerogen under Typical Reservoir Conditions. *Microporous Mesoporous Mater.* **2014**, *197*, 194–203. https://doi.org/10.1016/j.micromeso.2014.06.016.

(38) Collell, J.; Galliero, G.; Vermorel, R.; Ungerer, P.; Yiannourakou, M.; Montel, F.; Pujol, M. Transport of Multicomponent Hydrocarbon Mixtures in Shale Organic Matter by Molecular Simulations. *J. Phys. Chem. C* **2015**, *119* (39), 22587–22595. https://doi.org/10.1021/acs.jpcc.5b07242.

(39) Collell, J.; Ungerer, P.; Galliero, G.; Yiannourakou, M.; Montel, F.; Pujol, M. Molecular Simulation of Bulk Organic Matter in Type II Shales in the Middle of the Oil Formation Window. *Energy Fuels* **2014**, *28* (12), 7457–7466. https://doi.org/10.1021/ef5021632.

(40) Sui, H.; Yao, J. Effect of Surface Chemistry for CH4/CO2 Adsorption in Kerogen: A Molecular Simulation Study. *J. Nat. Gas Sci. Eng.* **2016**, *31*, 738–746. https://doi.org/10.1016/j.jngse.2016.03.097.

(41) Yiannourakou, M.; Ungerer, P.; Leblanc, B.; Rozanska, X.; Saxe, P.; Vidal-Gilbert, S.; Gouth, F.; Montel, F. Molecular Simulation of Adsorption in Microporous Materials. *Oil Gas Sci. Technol. – Rev. D'IFP Energ. Nouv.* **2013**, *68* (6), 977–994. https://doi.org/10.2516/ogst/2013134.

(42) Lee, T.; Bocquet, L.; Coasne, B. Activated Desorption at Heterogeneous Interfaces and Long-Time Kinetics of Hydrocarbon Recovery from Nanoporous Media. *Nat. Commun.* **2016**, *7*, 11890. https://doi.org/10.1038/ncomms11890.

(43) Ambrose, R. J.; Hartman, R. C.; Diaz-Campos, M.; Akkutlu, I. Y.; Sondergeld, C. H. Shale Gas-in-Place Calculations Part I: New Pore-Scale Considerations. *SPE J.* **2012**, *17* (01), 219–229. https://doi.org/10.2118/131772-PA.

(44) Wang, S.; Javadpour, F.; Feng, Q. Molecular Dynamics Simulations of Oil Transport through Inorganic Nanopores in Shale. *Fuel* **2016**, *171*, 74–86. https://doi.org/10.1016/j.fuel.2015.12.071.

(45) Wang, S.; Feng, Q.; Javadpour, F.; Yang, Y.-B. Breakdown of Fast Mass Transport of Methane through Calcite Nanopores. *J. Phys. Chem. C* **2016**, *120* (26), 14260–14269. https://doi.org/10.1021/acs.jpcc.6b05511.

(46) Zheng, H.; Du, Y.; Xue, Q.; Zhu, L.; Li, X.; Lu, S.; Jin, Y. Surface Effect on Oil Transportation in Nanochannel: A Molecular Dynamics Study. *Nanoscale Res. Lett.* **2017**, *12* (1), 413. https://doi.org/10.1186/s11671-017-2161-2.

(47) Underwood, T.; Erastova, V.; Cubillas, P.; Greenwell, H. C. Molecular Dynamic Simulations of Montmorillonite–Organic Interactions under Varying Salinity: An Insight into Enhanced Oil Recovery. *J. Phys. Chem. C* **2015**, *119* (13), 7282–7294. https://doi.org/10.1021/acs.jpcc.5b00555.

(48) Liu, Q.; Yuan, S.; Yan, H.; Zhao, X. Mechanism of Oil Detachment from a Silica Surface in Aqueous Surfactant Solutions: Molecular Dynamics Simulations. *J. Phys. Chem. B* **2012**, *116* (9), 2867–2875. https://doi.org/10.1021/jp2118482.

(49) Kästner, J. Umbrella Sampling. *Wiley Interdiscip. Rev. Comput. Mol. Sci.* **2011**, *1* (6), 932–942. https://doi.org/10.1002/wcms.66.

(50) Hughey, C. A.; Rodgers, R. P.; Marshall, A. G.; Qian, K.; Robbins, W. K. Identification of Acidic NSO Compounds in Crude Oils of Different Geochemical Origins by Negative Ion Electrospray Fourier Transform Ion Cyclotron Resonance Mass Spectrometry. *Org. Geochem.* **2002**, *33* (7), 743–759. https://doi.org/10.1016/S0146-6380(02)00038-4.

(51) Hyne, N. J. *Nontechnical Guide to Petroleum Geology, Exploration, Drilling, and Production*; PennWell Corporation: Tulsa, Okla., 2012.

(52) Jarvie, D. M. Shale Resource Systems for Oil and Gas: Part 2—Shale-Oil Resource Systems. **2012**, 89–119. https://doi.org/10.1306/13321447M973489.
(53) Buckley, J. S.; Liu, Y.; Monsterleet, S. Mechanisms of Wetting Alteration by Crude Oils. *SPE J.* **1998**, *3* (01), 54–61. https://doi.org/10.2118/37230-PA.
(54) Sayyouh, M. H.; Hemeida, A. M.; Al-Blehed, M. S.; Desouky, S. M. Role of Polar Compounds in Crude Oils on Rock Wettability. *J. Pet. Sci. Eng.* **1991**, *6* (3), 225–233. https://doi.org/10.1016/0920-4105(91)90015-F.
(55) Speight, J. G. The Chemical and Physical Structure of Petroleum: Effects on Recovery Operations. *J. Pet. Sci. Eng.* **1999**, *22* (1), 3–15. https://doi.org/10.1016/S0920-4105(98)00051-5.
(56) Composition, Classification, and Properties of Petroleum. In *Chemistry of Fossil Fuels and Biofuels*; Schobert, H., Ed.; Cambridge Series in Chemical Engineering; Cambridge University Press: Cambridge, 2013; pp 174–191. https://doi.org/10.1017/CBO9780511844188.012.
(57) Mango, F. D. The Light Hydrocarbons in Petroleum: A Critical Review. *Org. Geochem.* **1997**, *26* (7), 417–440. https://doi.org/10.1016/S0146-6380(97)00031-4.
(58) Yanik, J.; Yüksel, M.; Sağlam, M.; Olukçu, N.; Bartle, K.; Frere, B. Characterization of the Oil Fractions of Shale Oil Obtained by Pyrolysis and Supercritical Water Extraction. *Fuel* **1995**, *74* (1), 46–50. https://doi.org/10.1016/0016-2361(94)P4329-Z.
(59) Kvashnin, D. G.; Antipina, L. Y.; Sorokin, P. B.; Tenne, R.; Golberg, D. Theoretical Aspects of WS2 Nanotube Chemical Unzipping. *Nanoscale* **2014**, *6* (14), 8400–8404. https://doi.org/10.1039/C4NR00437J.
(60) Folk, R. L. *Petrology of Sedimentary Rocks*; Hemphill Publishing Company, 1980.
(61) Kerisit, S.; Parker, S. C. Free Energy of Adsorption of Water and Metal Ions on the {10$\bar{1}$4} Calcite Surface. *J. Am. Chem. Soc.* **2004**, *126* (32), 10152–10161. https://doi.org/10.1021/ja0487776.
(62) Curtis, J. B. Fractured Shale-Gas Systems. *AAPG Bull.* **2002**, *86* (11), 1921–1938. https://doi.org/10.1306/61EEDDBE-173E-11D7-8645000102C1865D.
(63) Jarvie, D. M.; Hill, R. J.; Ruble, T. E.; Pollastro, R. M. Unconventional Shale-Gas Systems: The Mississippian Barnett Shale of North-Central Texas as One Model for Thermogenic Shale-Gas Assessment. *AAPG Bull.* **2007**, *91* (4), 475–499. https://doi.org/10.1306/12190606068.
(64) Vandenbroucke, M.; Largeau, C. Kerogen Origin, Evolution and Structure. *Org. Geochem.* **2007**, *38* (5), 719–833. https://doi.org/10.1016/j.orggeochem.2007.01.001.
(65) Hu, Y.; Devegowda, D.; Striolo, A.; Phan, A.; Ho, T. A.; Civan, F.; Sigal, R. F. Microscopic Dynamics of Water and Hydrocarbon in Shale-Kerogen Pores of Potentially Mixed Wettability. *SPE J.* **2014**, *20* (01), 112–124. https://doi.org/10.2118/167234-PA.
(66) Firouzi, M.; Rupp, E. C.; Liu, C. W.; Wilcox, J. Molecular Simulation and Experimental Characterization of the Nanoporous Structures of Coal and Gas Shale. *Int. J. Coal Geol.* **2014**, *121*, 123–128. https://doi.org/10.1016/j.coal.2013.11.003.
(67) Falk, K.; Pellenq, R.; Ulm, F. J.; Coasne, B. Effect of Chain Length and Pore Accessibility on Alkane Adsorption in Kerogen. *Energy Fuels* **2015**, *29* (12), 7889–7896. https://doi.org/10.1021/acs.energyfuels.5b02015.
(68) Ambrose, R. J.; Hartman, R. C.; Diaz Campos, M.; Akkutlu, I. Y.; Sondergeld, C. New Pore-Scale Considerations for Shale Gas in Place Calculations; Society of Petroleum Engineers, 2010. https://doi.org/10.2118/131772-MS.
(69) Orendt, A. M.; Pimienta, I. S. O.; Badu, S. R.; Solum, M. S.; Pugmire, R. J.; Facelli, J. C.; Locke, D. R.; Chapman, K. W.; Chupas, P. J.; Winans, R. E. Three-Dimensional Structure of the Siskin Green River Oil Shale Kerogen Model: A Comparison between Calculated and Observed Properties. *Energy Fuels* **2013**, *27* (2), 702–710. https://doi.org/10.1021/ef3017046.

(70) Bousige, C.; Ghimbeu, C. M.; Vix-Guterl, C.; Pomerantz, A. E.; Suleimenova, A.; Vaughan, G.; Garbarino, G.; Feygenson, M.; Wildgruber, C.; Ulm, F.-J.; et al. Realistic Molecular Model of Kerogen's Nanostructure. *Nat. Mater.* **2016**, *15* (5), 576–582. https://doi.org/10.1038/nmat4541.

(71) Pei, Q.-X.; Zhang, Y.-W.; Shenoy, V. B. Mechanical Properties of Methyl Functionalized Graphene: A Molecular Dynamics Study. *Nanotechnology* **2010**, *21* (11), 115709. https://doi.org/10.1088/0957-4484/21/11/115709.

(72) Lee, S. S.; Heberling, F.; Sturchio, N. C.; Eng, P. J.; Fenter, P. Surface Charge of the Calcite (104) Terrace Measured by Rb+ Adsorption in Aqueous Solutions Using Resonant Anomalous X-Ray Reflectivity. *J. Phys. Chem. C* **2016**, *120* (28), 15216–15223. https://doi.org/10.1021/acs.jpcc.6b04364.

(73) Wolthers, M.; Tommaso, D. D.; Du, Z.; Leeuw, N. H. de. Calcite Surface Structure and Reactivity: Molecular Dynamics Simulations and Macroscopic Surface Modelling of the Calcite –Water Interface. *Phys. Chem. Chem. Phys.* **2012**, *14* (43), 15145–15157. https://doi.org/10.1039/C2CP42290E.

(74) Berendsen, H. J. C.; van der Spoel, D.; van Drunen, R. GROMACS: A Message-Passing Parallel Molecular Dynamics Implementation. *Comput. Phys. Commun.* **1995**, *91* (1), 43–56. https://doi.org/10.1016/0010-4655(95)00042-E.

(75) Robertson, M. J.; Tirado-Rives, J.; Jorgensen, W. L. Improved Peptide and Protein Torsional Energetics with the OPLS-AA Force Field. *J. Chem. Theory Comput.* **2015**, *11* (7), 3499–3509. https://doi.org/10.1021/acs.jctc.5b00356.

(76) Berendsen, H. J. C.; Postma, J. P. M.; van Gunsteren, W. F.; Hermans, J. Interaction Models for Water in Relation to Protein Hydration. In *Intermolecular Forces: Proceedings of the Fourteenth Jerusalem Symposium on Quantum Chemistry and Biochemistry Held in Jerusalem, Israel, April 13–16, 1981*; Pullman, B., Ed.; The Jerusalem Symposia on Quantum Chemistry and Biochemistry; Springer Netherlands: Dordrecht, 1981; pp 331–342. https://doi.org/10.1007/978-94-015-7658-1_21.

(77) Raiteri, P.; Gale, J. D.; Quigley, D.; Rodger, P. M. Derivation of an Accurate Force-Field for Simulating the Growth of Calcium Carbonate from Aqueous Solution: A New Model for the Calcite−Water Interface. *J. Phys. Chem. C* **2010**, *114* (13), 5997–6010. https://doi.org/10.1021/jp910977a.

(78) Geissbühler, P.; Fenter, P.; DiMasi, E.; Srajer, G.; Sorensen, L. B.; Sturchio, N. C. Three-Dimensional Structure of the Calcite–Water Interface by Surface X-Ray Scattering. *Surf. Sci.* **2004**, *573* (2), 191–203. https://doi.org/10.1016/j.susc.2004.09.036.

(79) Wolf, G.; Lerchner, J.; Schmidt, H.; Gamsjäger, H.; Königsberger, E.; Schmidt, P. Thermodynamics of CaCO3 Phase Transitions. *J. Therm. Anal. Calorim.* **1996**, *46* (2), 353–359. https://doi.org/10.1007/BF02135013.

(80) Wolf, G.; Königsberger, E.; Schmidt, H. G.; Königsberger, L.-C.; Gamsjäger, H. Thermodynamic Aspects of the Vaterite-Calcite Phase Transition. *J. Therm. Anal. Calorim.* **2000**, *60* (2), 463–472. https://doi.org/10.1023/A:1010114131577.

(81) Humphrey, W.; Dalke, A.; Schulten, K. VMD: Visual Molecular Dynamics. *J. Mol. Graph.* **1996**, *14* (1), 33–38. https://doi.org/10.1016/0263-7855(96)00018-5.

(82) Kumar, S.; Rosenberg, J. M.; Bouzida, D.; Swendsen, R. H.; Kollman, P. A. THE Weighted Histogram Analysis Method for Free-Energy Calculations on Biomolecules. I. The Method. *J. Comput. Chem.* **1992**, *13* (8), 1011–1021. https://doi.org/10.1002/jcc.540130812.

(83) Roux, B. The Calculation of the Potential of Mean Force Using Computer Simulations. *Comput. Phys. Commun.* **1995**, *91* (1), 275–282. https://doi.org/10.1016/0010-4655(95)00053-I.

(84) Hub, J. S.; de Groot, B. L.; van der Spoel, D. G_wham—A Free Weighted Histogram Analysis Implementation Including Robust Error and Autocorrelation Estimates. *J. Chem. Theory Comput.* **2010**, *6* (12), 3713–3720. https://doi.org/10.1021/ct100494z.
(85) Cleveland, W. S. Robust Locally Weighted Regression and Smoothing Scatterplots. *J. Am. Stat. Assoc.* **1979**, *74* (368), 829–836. https://doi.org/10.1080/01621459.1979.10481038.
(86) R Core Team. *R: A Language and Environment for Statistical Computing*; R Foundation for Statistical Computing: Vienna, Austria, 2019.
(87) Hakim, S. S.; Olsson, M. H. M.; Sørensen, H. O.; Bovet, N.; Bohr, J.; Feidenhans'l, R.; Stipp, S. L. S. Interactions of the Calcite {10.4} Surface with Organic Compounds: Structure and Behaviour at Mineral – Organic Interfaces. *Sci. Rep.* **2017**, *7* (1), 7592. https://doi.org/10.1038/s41598-017-06977-4.
(88) Ross, D. J. K.; Bustin, R. M. Shale Gas Potential of the Lower Jurassic Gordondale Member, Northeastern British Columbia, Canada. *Bull. Can. Pet. Geol.* **2007**, *55* (1), 51–75. https://doi.org/10.2113/gscpgbull.55.1.51.
(89) Loucks, R. G.; Reed, R. M.; Ruppel, S. C.; Jarvie, D. M. Morphology, Genesis, and Distribution of Nanometer-Scale Pores in Siliceous Mudstones of the Mississippian Barnett Shale. *J. Sediment. Res.* **2009**, *79* (12), 848–861. https://doi.org/10.2110/jsr.2009.092.
(90) Madsen, L.; Grahl-Madsen, L.; Grøn, C.; Lind, I.; Engell, J. Adsorption of Polar Aromatic Hydrocarbons on Synthetic Calcite. *Org. Geochem.* **1996**, *24* (12), 1151–1155. https://doi.org/10.1016/S0146-6380(96)00096-4.
(91) García Carmona, J.; Gómez Morales, J.; Rodríguez Clemente, R. Rhombohedral–Scalenohedral Calcite Transition Produced by Adjusting the Solution Electrical Conductivity in the System Ca(OH)2–CO2–H2O. *J. Colloid Interface Sci.* **2003**, *261* (2), 434–440. https://doi.org/10.1016/S0021-9797(03)00149-8.
(92) Shen, J.-W.; Li, C.; van der Vegt, N. F. A.; Peter, C. Understanding the Control of Mineralization by Polyelectrolyte Additives: Simulation of Preferential Binding to Calcite Surfaces. *J. Phys. Chem. C* **2013**, *117* (13), 6904–6913. https://doi.org/10.1021/jp402341w.

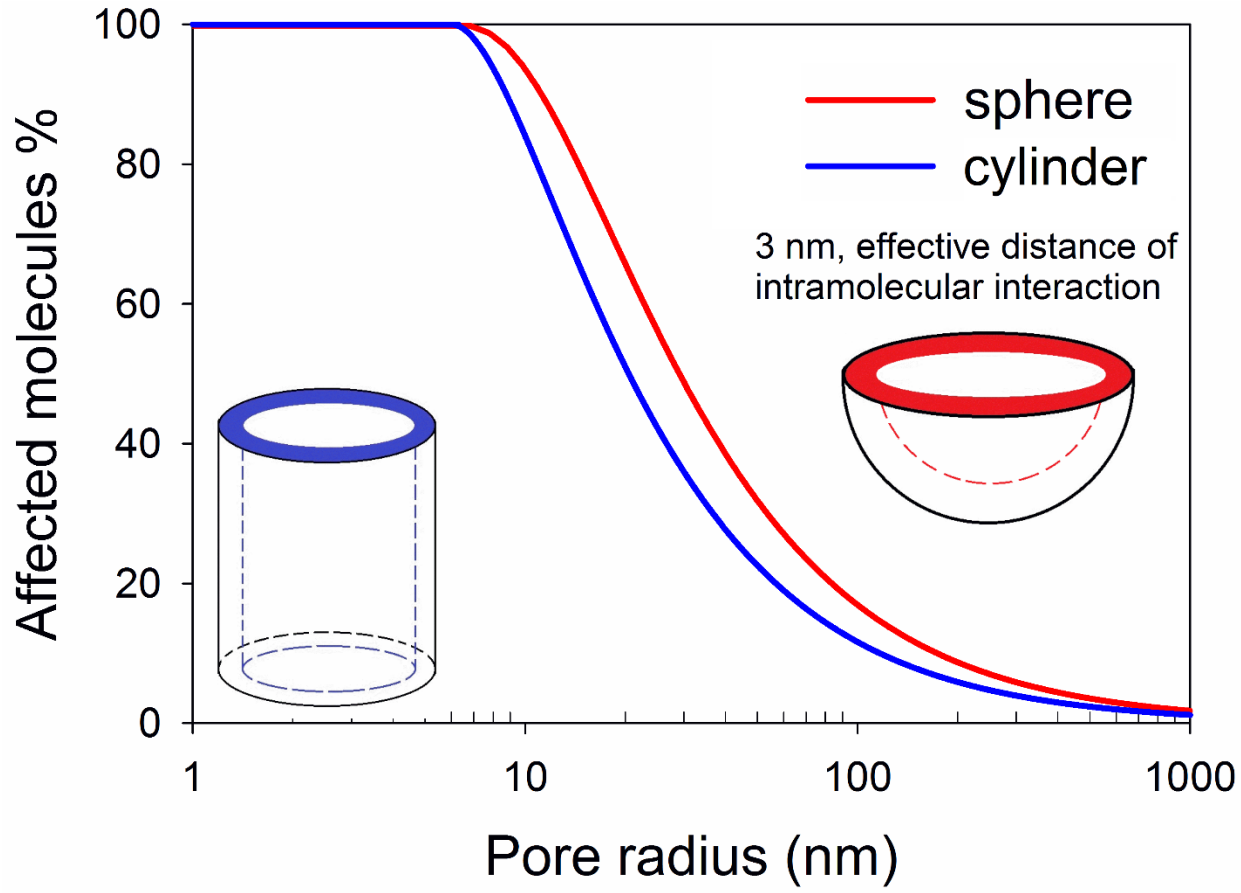

Figure 1. Effect of intermolecular interaction on the fluid confined in nanostructures.

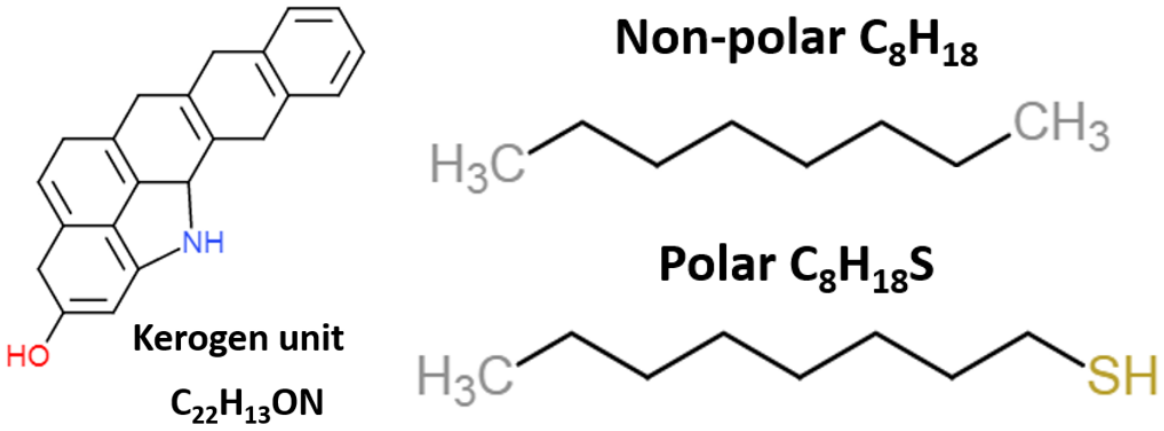

Figure 2. Molecular structure of type II kerogen fragment (left), non-polar oil n-octane (right top), and polar oil 1-octanethiol (right bottom).

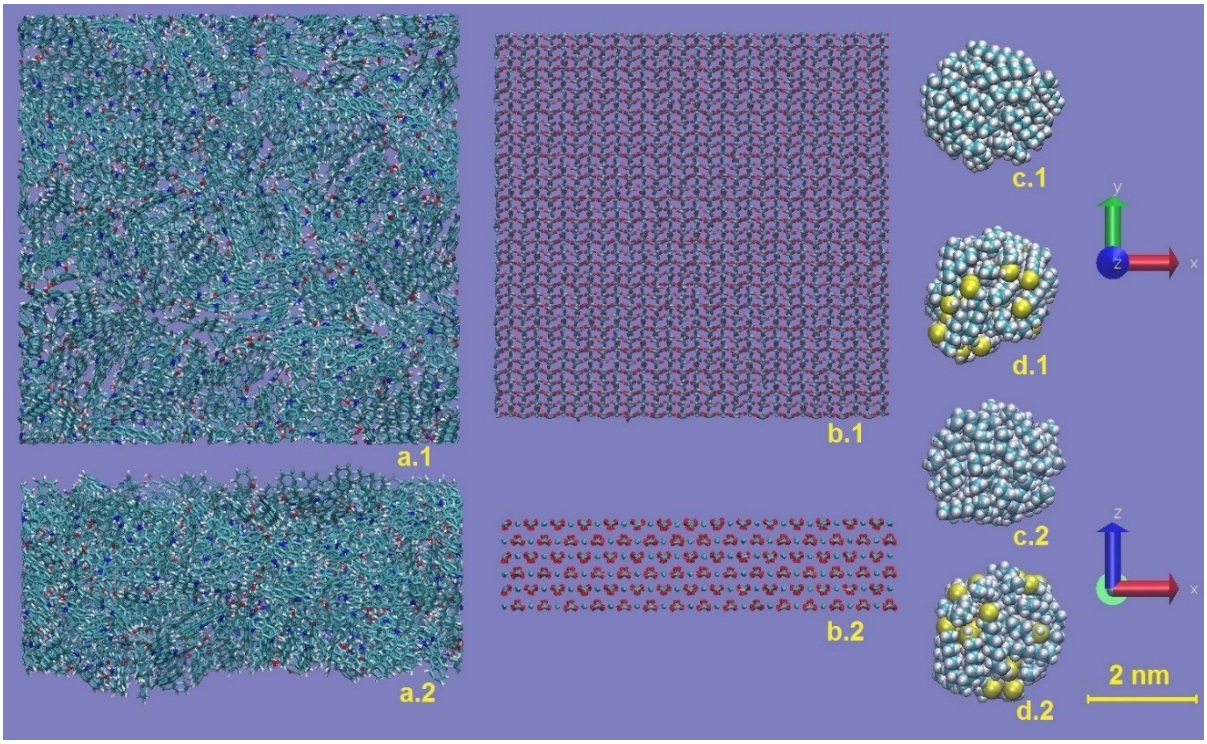

Figure 3. Kerogen slab (a), calcite (104) slab (b), 30-molecule non-polar oil cluster (c), and 30-molecule polar oil cluster (d). "x.1" and "x.2" denote different orientations.

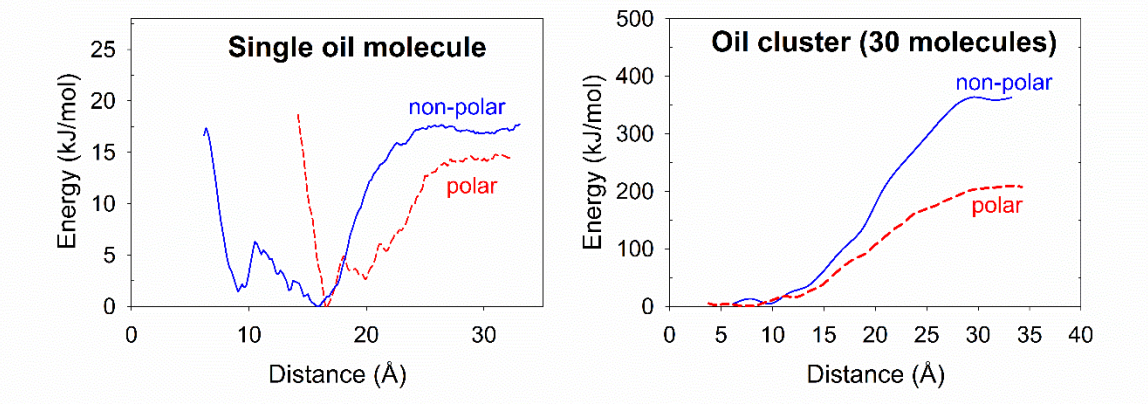

630

631 Figure 4. Free energy surfaces of single molecule of polar or non-polar oil on kerogen surface with water
632 (left); Free energy surfaces of oil drop of 30 polar or non-polar oil molecules on kerogen surface with
633 water (right).

634

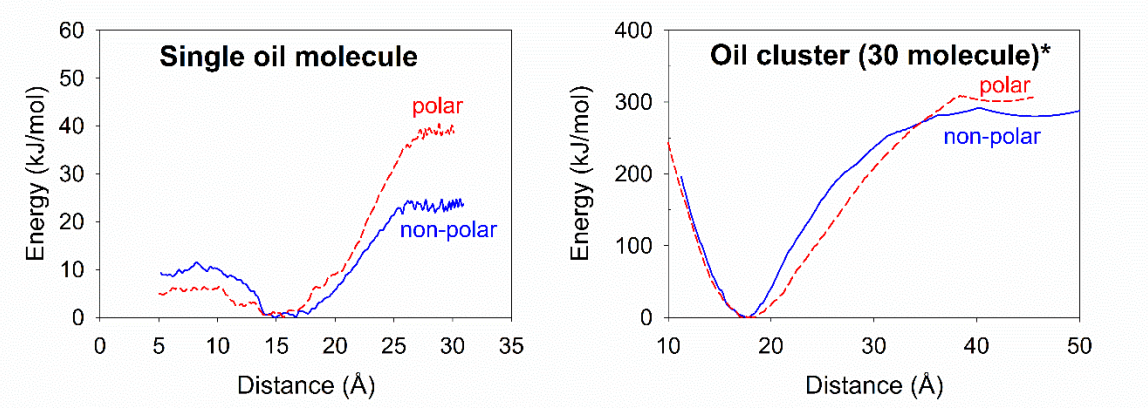

Figure 5. Free energy surfaces of single molecule of polar and non-polar oil on kerogen surface without water (left); free energy surfaces of oil drop of 30 polar or non-polar oil molecules on kerogen surface without water (right). *indicates the simulations were prepared at 200K due to the technical issues as described in the discussion.

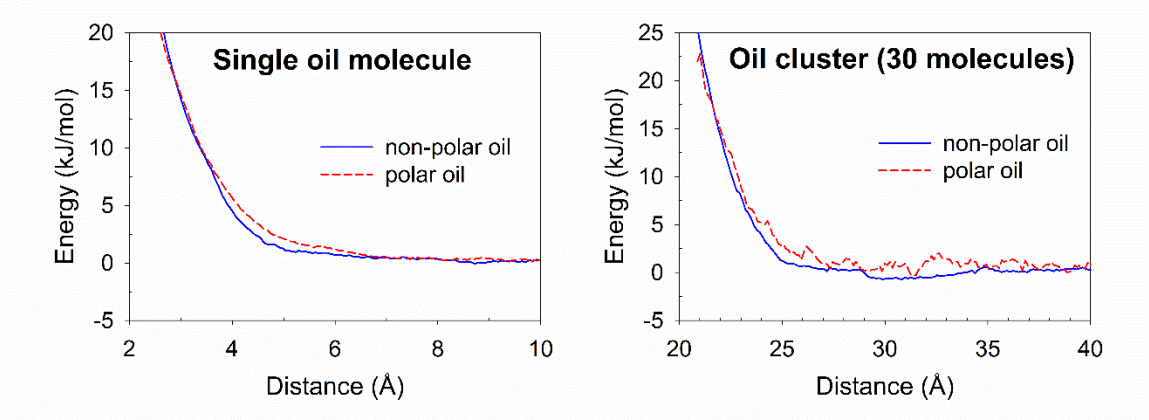

641

642 Figure 6. Free energy surfaces of single molecule and 30-molecule cluster of polar or non-polar oil on
643 calcite surface in the presence of water.

644

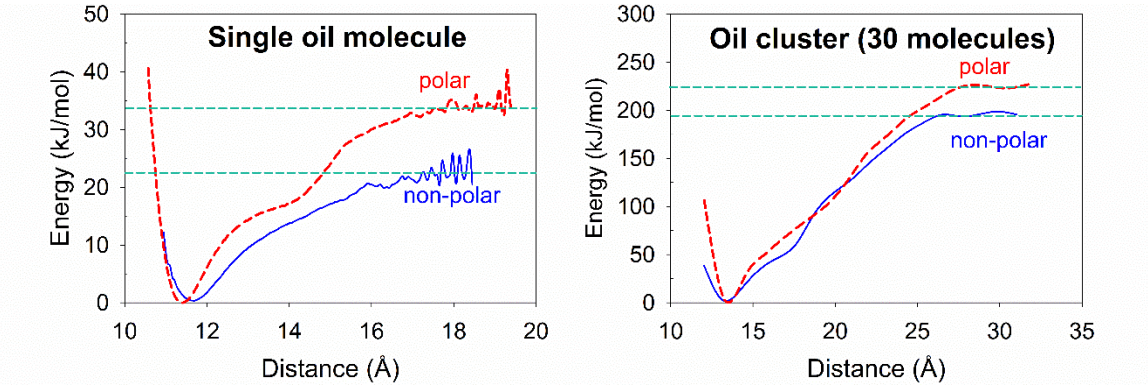

Figure 7. Free energy surfaces of single molecule of polar or non-polar oil on calcite surface without water (left); free energy surfaces of oil drop of polar or non-polar oil on calcite surface without water (right).

650

Table 1. Desorption energy of single molecule oil droplet and 30-molecule oil drop on calcite and kerogen surface under 300 K. The ( ) denotes the errors propagated from the output data of WHAM.

Desorption energy (kJ/mol)		Kerogen with water	Kerogen	Calcite with water	Calcite
Non-polar oil	Single molecule	17.0 (2.0)	23.3 (3.5)	0	18.0 (5.5)
	Cluster - total	372 (13.8)	438 (13. 5)	0	198 (42)
	Cluster - per molecule	12.4 (0.46)	14.6 (0.45)	0	6.6 (1.4)
Polar oil	Single molecule	16.5 (3.3)	39.5 (9.5)	0	33.6 (3.9)
	Cluster - total	210 (11.4)	438 (13.5)	0	222 (36)
	Cluster - per molecule	7.0 (0.38)	14.6 (0.45)	0	7.4 (1.2)

651 **Supplement Information**
652

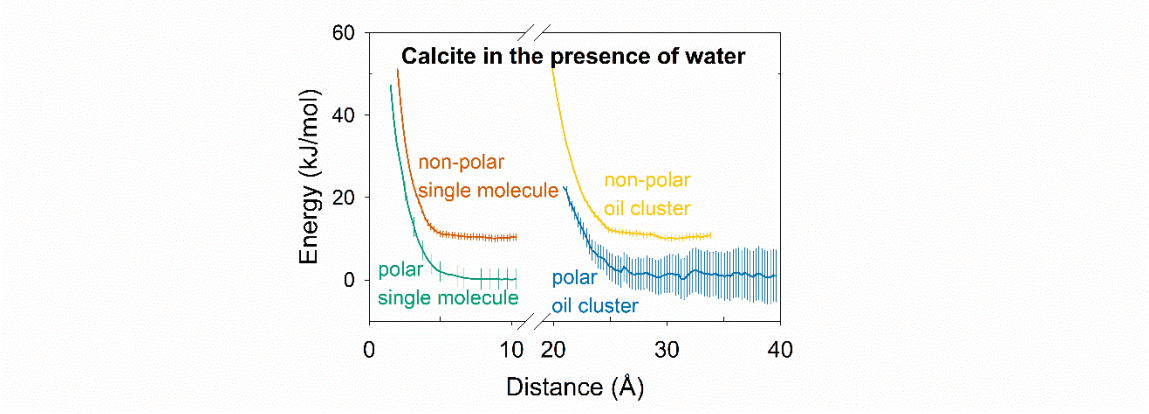

653

654 Figure S1. Free energy surfaces of oil drop of polar or non-polar oil on calcite surface with water. The
655 density of displayed data is reduced for visual clarity.

656

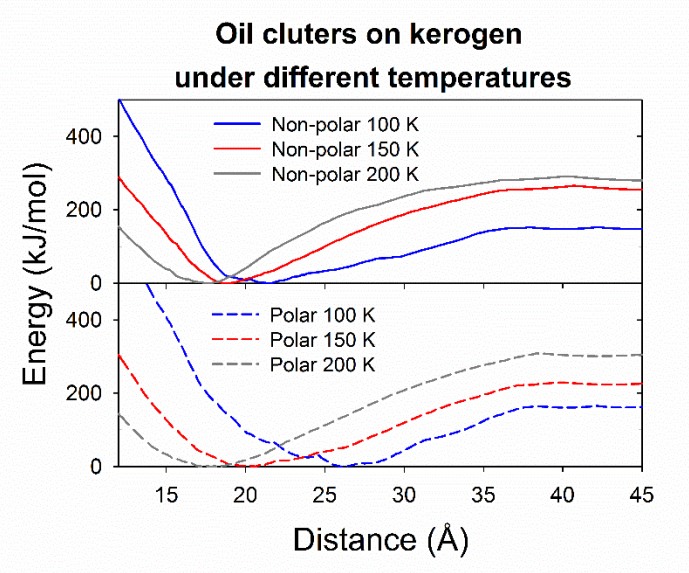

Figure S2. Free energy surfaces of 30-molecule oil drops interacting with kerogen surface under different temperatures. According to the data point pattern on this chart, the correlation between desorption energy and temperature can be formulated using the same equation below for both polar and non-polar oil. The error bars are smaller than the symbol size.

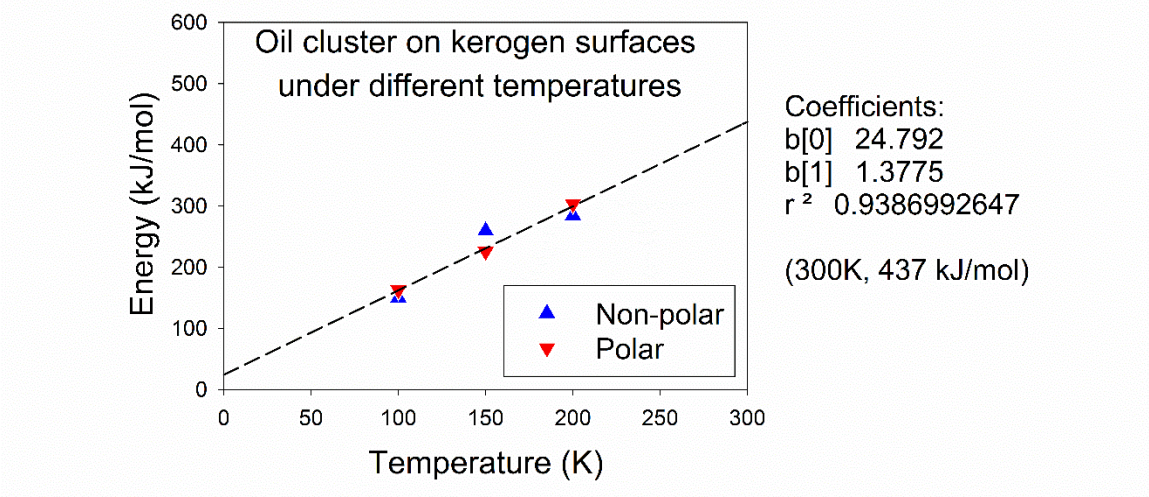

Figure S3. Desorption energies of 30-molecule oil drops on kerogen surfaces under different temperatures.

The non-polar and polar oil drops exhibit linear relationship between temperature and desorption energy (with a R-squared value of 0.9387). The non-polar and polar oil drops follow the same correlation between desorption energy (E_d in kJ/mol) and temperature (T in K):

$$E_d = 1.38 \cdot T + 24.8$$

The energy required for oil drop desorption from kerogen surface increases when the system temperature rises. As shown in Figure S5, a close examination on the interface of oil and surface reveals that oil molecule is strongly attached to the kerogen surface. The same correlation of energy and temperature suggested that the intermolecular bonding between kerogen and oil are so strong that the effect of oil polarity is negligible in such interactions.

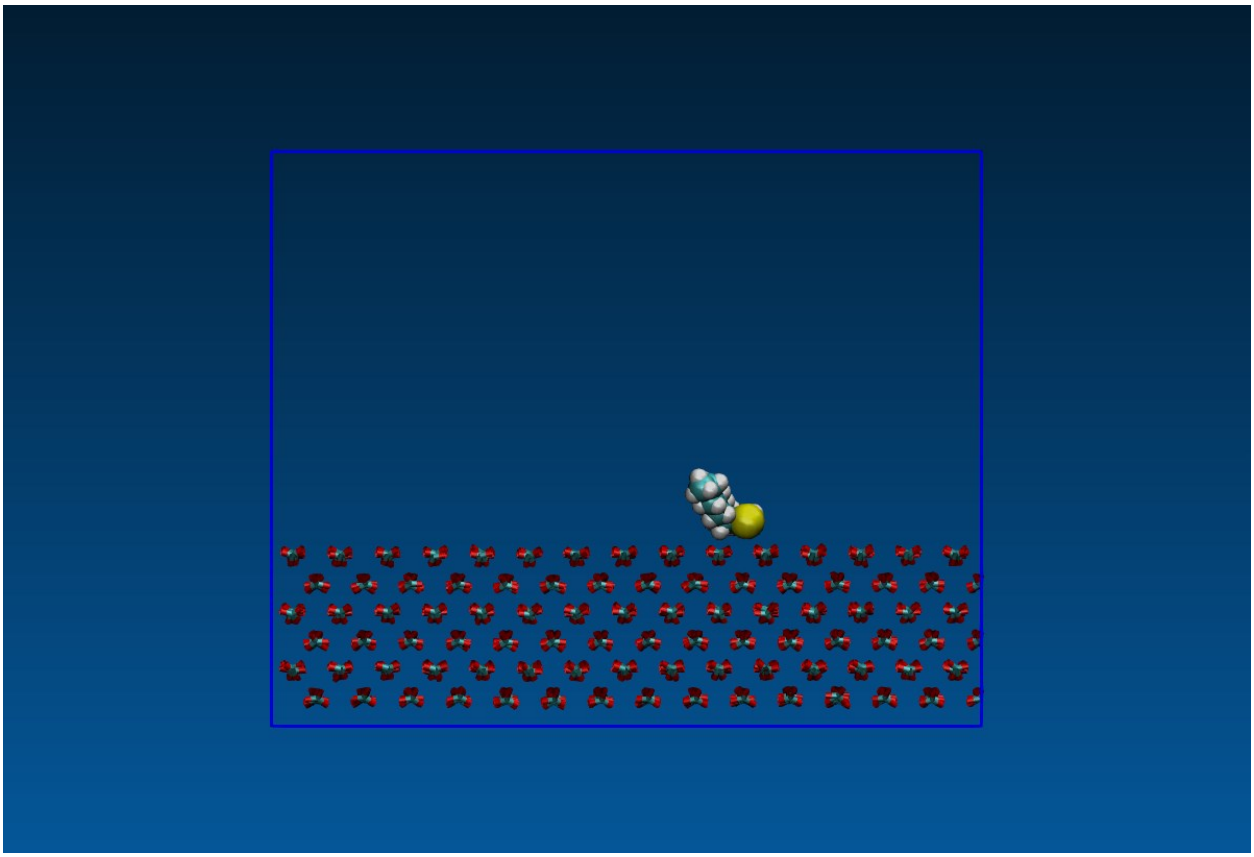

Figure S4. Snapshot of the simulation trajectory of calcite surface interaction with polar oil molecule in the absence of water.

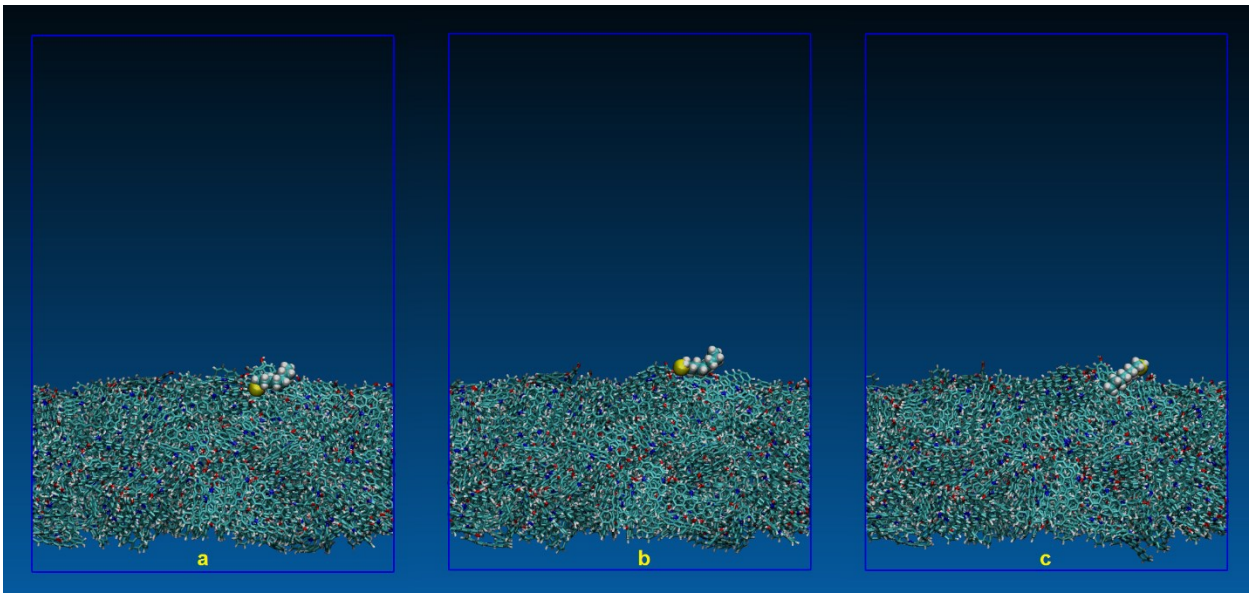

Figure S5. Snapshot of the simulation trajectory of kerogen surface interaction with polar oil molecule in the absence of water at different time step. (a) and (b) depict strong interactions between polar oil functional group –SH and kerogen functional groups –NH– and –OH, whereas (c) illustrates strong interactions between non-polar carbon chain of polar oil and non-polar benzene rings of kerogen.

690 Table S1. Desorption energies of oil drops on kerogen surface under different temperatures in the absence
691 of water.

Desorption energy in kJ/mol [error]		
Temperature	Non-polar	Polar
100 K	150.5 [2.5]	163 [3]
150 K	260 [5.5]	226 [3]
200 K	285 [5.5]	304 [5]

692

693

Code for error estimation (Anaconda RStudio 1.1.456)

```
library(bootstrap)
attach(dat)

B<-150
boot.fit<-matrix(0,B,length(x))

for (i in 1:B){
set.seed(i)
indx <- sample(1:178,size=178,replace=T)

fit <- loess(y~x,dat[indx,],span=0.30)

boot.fit[i,] <- predict(fit,x)
}

FUN<-function(x){
quantile(x,prob=c(.025,.975),na.rm=T)  # calcutlate 95% CI
}
boot.CI<-apply(boot.fit,2,FUN)

y_2.5<-boot.CI[1,]
y_97.5<-boot.CI[2,]
```